FORM TI-12
07/1999

B-T-3337

EFFECT OF MICROSTRUCTURE ON LOW TEMPERATURE CRACKING BEHAVIOR OF EN82H WELDS

W. J. Mills, C. M. Brown and M. G. Burke

May 2001

DE-AC11-98PN38206

BETTIS ATOMIC POWER LABORATORY WEST MIFFLIN, PENNSYLVANIA 15122-0079

Operated for the U.S. Department of Energy
by Bechtel Bettis, Inc.

Effect of Microstructure on Low Temperature Cracking Behavior of EN82H Welds

W. J. Mills, C. M. Brown, and M. G. Burke

Bettis Atomic Power Laboratory
West Mifflin, Pennsylvania 15122

ABSTRACT

As-fabricated EN82H welds are susceptible to low temperature embrittlement in 54°C hydrogenated water. Values of J_{IC} in water are typically 90% to 98% lower than those in air due to a fracture mechanism transition from microvoid coalescence to hydrogen-induced intergranular fracture. Environmental J_{IC} testing demonstrated that a high temperature (1093°C) anneal and furnace-cool alleviates the material's susceptibility to hydrogen-induced intergranular cracking. To identify metallurgical and compositional features that are responsible for the material's environment-sensitive behavior, detailed characterization of the microstructure and grain boundary chemistry for the as-fabricated and as-annealed materials was performed. Results from light optical microscopy, analytical electron microscopy, electron probe microanalysis, Auger electron spectroscopy and mechanical property characterization are used to provide insight into the observed low temperature embrittlement phenomenon. The key microstructural feature responsible for low temperature cracking in as-fabricated welds appears to be fine niobium and titanium-rich carbonitrides that cover most grain boundaries. These precipitates are effective hydrogen traps that promote hydrogen-induced intergranular cracking. Dissolution of the fine carbonitrides during the 1093°C anneal reduces grain boundary trapping sites, which accounts for the improved fracture resistance displayed by the annealed weld. The role of strength level in promoting low temperature embrittlement is evaluated by cold-rolling the annealed weld to increase its yield strength from 280 to 640 MPa. The annealed and cold-rolled weld exhibits high toughness in 54°C water and shows no evidence of hydrogen-induced intergranular cracking, thereby demonstrating that strength is not a primary cause of low temperature embrittlement.

INTRODUCTION

Alloy 600 components used in commercial primary water reactors are often welded using EN82H weld metal and similar nickel-base alloys, such as Alloy 182 weld metal. When subjected to high temperature water these materials are susceptible to stress corrosion cracking (SCC).[1-3] Crack growth rates in weld metals are highly variable and can be significantly greater than their base metal counterpart. In addition, the fracture resistance of as-fabricated EN82H welds is severely degraded in low temperature water due to a hydrogen-induced intergranular cracking mechanism. [4,5]

The exceptionally high toughness displayed by EN82H welds in air and high temperature water demonstrates that fracture is not expected under these conditions. However, fracture is a concern in low temperature, hydrogenated water, as J_{IC} values and tearing moduli are reduced by 90% to 98%. Decreasing the hydrogen concentration from 150 to 15 cc H_2/kg H_2O causes a relatively small improvement in low temperature crack propagation (LTCP) resistance.[5] The degree of embrittlement is relatively insensitive to water temperature below 100°C, but significant toughness is restored at 150°C.[4]

The dramatic toughness degradation in low temperature water is associated with a fracture mechanism transition from ductile dimple rupture to intergranular cracking. In air and high temperature water, extensive plastic deformation is required to initiate and grow microvoids and create shear-stretch zones. The latter mechanism is produced by an alternating shear rupture process that operates when large shear stresses develop in ligaments between adjacent microvoids. In low temperature water, intergranular cracking is dominant and there is evidence of localized islands of crystallographic faceting. The degree of embrittlement and intergranular cracking mechanisms observed in low temperature water were reproduced in hydrogen-precharged specimens tested in air. This finding demonstrates that low temperature crack propagation (LTCP) is a hydrogen embrittlement mechanism. Hydrogen from the water not only weakens grain boundaries so they separate at low strain levels, it promotes a planar slip mechanism that localizes strain concentrations along grain boundaries.[4,5]

The current study shows that a 1093°C anneal and furnace-cool restores significant toughness in 54°C water and eliminates the propensity for intergranular cracking. This behavior offers a unique opportunity to study a given weld in the susceptible and nonsusceptible

conditions to identify the key parameters responsible for intergranular cracking in low temperature water. Therefore, a primary objective of this study is to characterize differences in the mechanical behavior and microstructure for an EN82H weld in the as-fabricated and annealed conditions. The evaluation program included J_{IC} testing in room temperature air and 54°C water, tension testing, light microscopy, scanning electron microscopy (SEM), analytical electron microscopy (AEM), electron probe microanalysis (EPMA) and Auger electron spectroscopy (AES). In addition, the effect of strength level on low temperature cracking susceptibility was characterized by conducting environmental J_{IC} tests on annealed and cold-rolled welds.

TEST MATERIAL AND EXPERIMENTAL PROCEDURES

The EN82H weld was fabricated by joining two Alloy 600 plates using a manual gas-tungsten-arc (GTA) weld process with a pure argon shield gas. The chemical composition (in weight percent) for this weld filler metal, identified as Weld "C5" in Reference (5), is 0.04% C, 2.93% Mn, 0.73% Fe, <0.001% S, 73.6% Ni, 19.8% Cr, 0.30% Ti, 0.004% P, and 2.51% Nb. Sections of weldments were evaluated in the as-fabricated condition, after annealing at 1093°C for 4 hours followed by furnace cooling, and in the 1093°C annealed and 15% cold-rolled condition.

Tension tests of round tension specimens with a gage length of 25 mm and gage diameter of 4.8 mm were conducted in ambient air at a nominal strain rate of 5×10^{-4} s^{-1}. Yield and ultimate strength levels were determined from load versus displacement records, and ductility values were obtained from pre- and post-test specimen measurements.

Fracture toughness tests were performed in 24°C air and 54°C water on precracked compact tension (CT) specimens with a width of 30.5 mm, thickness of 15.2 mm and 20% side grooves. Tests in water were conducted at a rate of 4 MPa$\sqrt{m}$/h to allow sufficient time for environmental effects to occur. The water environment had a room temperature pH of 10.1 to 10.3, an oxygen concentration between 3 and 17 ppb and a nominal hydrogen concentration of 150 cc H_2/kgH_2O. Fracture tests were conducted in accordance with J-R curve and J_{IC} normalization procedures.[5,6] Fracture properties reported herein include J_{IC}, the value of J at the onset of cracking, and tearing modulus (T), a dimensionless measure of a material's

resistance to tearing at J values above J_{IC}.[7] To determine operative cracking mechanisms, fracture surfaces of key specimens were characterized by scanning electron microscopy.

The microstructures for the as-fabricated and annealed welds were characterized by light optical microscopy (LOM), electron probe microanalysis (EPMA), SEM and AEM techniques. Thin-foil specimens were prepared for AEM studies by standard jet electropolishing techniques using an electrolyte of 20% HCl_4 – 80% CH_3OH at -40°C. Microstructural characterization was performed using a Philips CM12 analytical electron microscope operated at 120 kV and equipped with a LaB_6 cathode and a Link Analytical LZ_5 windowless energy dispersive x-ray spectrometer and an AN10/85S analyzer.

The grain boundary microchemistry was characterized by AES analysis of in-situ fracture surfaces on a Model 660 Scanning Auger Microscope manufactured by Physical Electronics Industries. Small cantilever bend specimens suitable for fracture in an AES high vacuum chamber were precharged with 55 to 60 ppm hydrogen. To assure a uniform hydrogen distribution, precharging was performed in high-pressure autoclaves at 360°C for six weeks. Samples were secured in the analysis vacuum chamber and fractured by slow bending immediately prior to AES examination. General survey spectra were obtained to show composition variations along grain boundaries. SEM fractographs from the interrogated regions were carefully reviewed to determine which analyses correspond to intergranular and transgranular fracture surfaces.

RESULTS

Tensile Properties

Room temperature tensile properties in Table 1 show that the weld used in this study has particularly high strength levels. Annealing at 1093°C is seen to significantly reduce strength and increase elongation. Table 1 also shows that cold rolling of the annealed weld increases the strength to levels that are slightly higher than those for the as-fabricated condition.

Fracture Behavior in Air and Water

The fracture toughness response for the EN82H weld tested in air and water is provided in Figure 1. The as-fabricated weld exhibits very high fracture toughness in air, with J_{IC} values of 953 and 1129 kJ/m^2 and tearing moduli of 296 and 435. In 54°C water the fracture

resistance is severely degraded as J_{IC} and T are reduced by 99% (J_{IC} = 13 kJ/m², T = 5). The loss in toughness is associated with a fracture mechanism transition from ductile dimple rupture to intergranular cracking (Figure 2a). This behavior is consistent with that reported in References (4) and (5).

The 1093°C annealed weld also exhibits exceptionally high toughness in air. Its J_{IC} of 955 kJ/m² is comparable to that for the as-welded condition, while its tearing modulus of 674 exceeds its as-welded counterpart. Although the toughness of the annealed weld is reduced in 54°C water (J_{IC} = 254-506 kJ/m² and T = 306-412), the degree of degradation is far less than that for the as-fabricated weld. In fact, the annealed weld retains sufficient toughness in low temperature water to eliminate fracture as a concern.

The fracture surface morphology for the annealed weld tested in 54°C water is markedly different than those for the as-fabricated weld tested in air or water. The fracture surface takes on a faceted appearance with no evidence of intergranular cracking, as shown in Figures 2b and 2c. Most of the facets are small, but a few are large and steeply inclined to the loading direction. The steep angle indicates that the faceting mechanism is dominated by shear stresses, which are maximized in this orientation. Some evidence of dimple rupture is observed, but the dimples are poorly defined. The faceted morphology is essentially the same as that observed in hydrogen-precharged Alloy 600 and within transgranular islands in hydrogen-precharged EN82H welds.[5] In the latter, transgranular faceting was found to occur in localized ligaments that resist intergranular cracking. After the primary intergranular crack extends well beyond these ligaments, local stress intensities become large enough to nucleate separation along planar slip bands, thereby resulting in the crystallographic facets. Reference (5) concluded that hydrogen in the matrix promotes heterogeneous deformation and separation along planar slip bands, except when preempted by hydrogen-induced intergranular cracking.

For the annealed weld tested in water, the presence of crystallographic facets indicates that the lattice picked up sufficient hydrogen from the water to induce planar slip and separation along slip bands after significant plastic deformation. This behavior accounts for the partial recovery in toughness after annealing. Moreover, the absence of intergranular cracking in a matrix that is embrittled by hydrogen indicates that the 1093°C anneal and slow cool alters the grain boundary morphology such that it resists hydrogen embrittlement.

It is noted that annealing at 1093°C alters the microstructure,[8] as discussed later, and reduces the yield strength from 620 to 280 MPa. Because strength level affects local hydrogen concentrations and stresses ahead of crack tips, it is possible that the absence of intergranular cracking in the annealed weld may be due to reduced strength levels (rather than differences in grain boundary structure). To evaluate this possibility, fracture toughness tests were performed on a section of weld that was annealed and then cold-rolled so its yield strength (640 MPa) was comparable to that for the as-fabricated weld. Figure 1 shows that cold rolling causes a modest reduction in fracture toughness in air as J_{IC} is reduced from 955 kJ/m² after annealing to 381-567 kJ/m² after annealing and cold rolling. In a similar fashion, cold working reduces T from 674 to 133-150. This response is expected because increased strength levels restrict plastic deformation capabilities. Low temperature water is seen to have relatively little effect on the toughness of the annealed and cold-rolled weld, as both J_{IC} and T in 54°C water are reduced by only 20%. The fracture surface for the annealed and cold-rolled weld tested in water is predominantly dimple rupture with limited evidence of large, steeply inclined facets (Figure 3).

General Microstructure Characterization:

Light Optical Microscopy and Scanning Electron Microscopy

LOM and SEM techniques were used to evaluate the general microstructure of the as-fabricated and annealed welds. Representative micrographs for both material conditions are shown in Figures 4 through 7.

As-fabricated weld – Figure 4 reveals that the as-fabricated weld exhibits well-defined grain boundaries separating colonies of similarly oriented dendrites. The grain structure is anisotropic, particularly in the weld root region where columnar grains are aligned normal to the welding direction. Numerous inclusions are observed in the interdendritic regions throughout the weld fusion zone (Figure 4b and 5a).

Unlike the polygonal-shaped boundaries present in wrought metals, grain boundaries in the weld have a wavy or curved shape, as shown in Figures 4 and 5a. This undulating appearance, which is typical of an as-welded structure, results from impingement of dendritic colonies and inclusions pinning grain boundaries along interdendritic regions. The wavy morphology gives rise to the undulating nature of intergranular fracture in as-fabricated welds, as shown in Figure 2a.

The SEM micrograph in Figure 5b also shows evidence of small, brightly-imaging precipitates decorating essentially all grain boundaries. These features appear to be agglomerated in this etched specimen.

Annealed weld – Annealing at 1093°C and slow cooling caused a change in microstructure from the cellular dendritic grains to equiaxed grains (Figure 6a) that varied from 20 to 400 μm in size. The high proportion of annealing twins present after solution annealing results from recrystallization of the as-welded microstructure.

Some regions of the annealed weld show what appears to be original grain boundaries (Figure 6b and 7a). In these regions, a columnar grain structure with wavy grain boundaries remains. Unrecrystallized grain boundaries in the annealed weld continue to exhibit coarsened intergranular precipitates, whereas no evidence of these precipitates is observed along recrystallized boundaries. Inclusions that formed in interdendritic regions are not dissolved during annealing as they are present in both the recrystallized and unrecrystallized regions.

Analytical Electron Microscopy

AEM characterization revealed significant microstructural differences between the as-fabricated and as-annealed weldments.[8]

As-fabricated weld – The as-fabricated weld was characterized by a heavily dislocated microstructure with a variety of dislocation tangles, planar arrays and dislocation networks. The general structure is shown in Figure 8.

Detailed characterization of the grain boundaries revealed that most boundaries in the as-fabricated weld were decorated with fine face-centered cubic (fcc) MC-type carbonitrides ranging from 3 to 16 nm in size. STEM-EDS microanalysis confirmed that these precipitates were enriched in Nb and Ti. Figure 9 contains typical examples of the discrete intergranular M(C,N) precipitates, which are incoherent with the fcc matrix. In addition to the intergranular precipitates, a nonuniform distribution of fine M(C,N) precipitates was observed throughout the matrix. The size and distribution of these precipitates indicated that they had nucleated on pre-existing dislocations, as shown in Figure 9b. The AEM analysis also provided evidence of coarse (~1 μm) TiN inclusions with AlMgSi-rich oxide inclusions. No Cr-rich $M_{23}C_6$ carbides or intergranular Cr depletion was detected in the weldment.

Annealed weld – The 1093°C anneal resulted in a dramatic reduction in dislocation content, consistent with a fully recrystallized microstructure. Some planar arrays of dislocations were occasionally observed in the vicinity of coarse inclusions, as expected for an as-cooled structure. Figure 10 shows the typical recrystallized microstructure associated with the annealed weld. AEM characterization confirmed that the 1093°C anneal dissolved the vast majority of the fine inter- and intragranular carbonitrides that were present in the as-fabricated weld. This high-temperature anneal promoted the intergranular precipitation of Cr-rich M_7C_3 (Figure 11a), and $M_{23}C_6$ on some boundaries (Figure 11b). The fcc $M_{23}C_6$ carbides exhibited the well-known cube-cube orientation relationship with the fcc weld matrix, and were semicoherent with the matrix.

AEM analysis showed that the pre-existing TiN and AlMgSi-rich oxide inclusions serve as heterogeneous nucleation sites for preferential precipitation of NbC during the 1093°C anneal and slow cool. Specifically, the AlMgSi-rich spheroidal oxide inclusions were observed to act as nucleation sites for the primary TiN inclusions, and appeared as a "core" within the TiN inclusions. During the 1093°C anneal and slow-cool, the Nb and Ti in solution formed the MC (predominantly NbC) carbides at the TiN/matrix interface. This resulted in the formation of the complex multi-phase inclusions shown in Figure 12. These inclusions were occasionally observed at grain boundaries, as they apparently pinned the migrating boundaries.

Some isolated regions were observed within the weld that had not recrystallized during the high-temperature anneal, as shown in Figure 13. These areas were characterized by an increased dislocation content and the presence of discrete Nb-rich carbonitrides that were notably coarser (up to 200 nm) than the ultra-fine carbonitrides present in the as-fabricated weld. The microstructure within these regions appeared to have experienced some degree of recovery of the heavily dislocated structure present in the as-welded condition, as evidenced by the presence of some subgrains.

Electron Probe Microanalysis

Wavelength dispersive x-ray linescans provided evidence of microsegregation and a cored structure with enriched Mn and Nb concentrations in interdendritic regions. Such microsegregation is typical for an as-welded microstructure.

The 1093°C anneal resulted in a significant reduction in microsegregation, as determined by EPMA measurement. Electron microprobe evaluations confirmed that the Nb and Mn partitioning had been eliminated, as compared with the microsegregation present within the as-fabricated weld.

Auger Electron Spectroscopy

Grain boundary compositions for as-fabricated and annealed EN82H welds are listed in Table 2. Auger results for transgranular cracked regions are also presented to provide a comparison for determining the degree of enrichment along grain boundaries. In the as-fabricated condition, there appears to be limited evidence of P segregation, but no evidence of S segregation. Six of the thirteen grain boundaries interrogated show little or no P segregation (0.6 ± 0.2 a/o), whereas seven boundaries show an average of 1.4 ± 0.3 atomic percent P, which is about 1 atomic percent higher than that in the transgranular regions. No evidence of P or S segregation was observed in the annealed weld.

The slightly elevated Mn levels for grain boundaries in the as-fabricated weld are probably associated with Mn enrichment in interdendritic regions. This is consistent with the EPMA data that showed increased concentrations of Mn and Nb in the periphery of cellular dendrites. It is noted that the considerable uncertainty in AES Mn measurements, as reflected by large standard deviations, is probably due to 1) a heterogeneous distribution of Mn in the interdendritic and intradendritic regions, and 2) overlap in Mn and Cr peaks.

AES spectra results in Table 2 together with the elemental distribution maps in Figure 14 show that grain boundaries in the as-fabricated weld are enriched in Nb, C and N (not mapped), consistent with AEM analysis showing the presence of fine intergranular niobium-rich carbonitrides. Table 2 reveals that there are two populations of grain boundaries, with some showing modest Nb and N enrichment (7.6 ± 2.4 a/o Nb, 1.5 ± 0.5 a/o N) and others showing greater enrichment (19.2 ± 2.0 a/o Nb, 2.5 ± 0.4 a/o N). The elemental maps indicate that grain boundaries with higher Nb enrichment also exhibit increased C enrichment. This boundary-to-boundary variability is consistent with grain boundaries being located in both interdendritic and intradendritic regions and varying densities of niobium-rich carbonititrides. In addition to Nb enrichment, Ti and Cr enrichments were also detected on some boundaries, suggesting that

there may be some Ti and Cr substitution for Nb. A few boundaries exhibit enriched Cr and C levels without increased Nb. This observation suggests that Cr-rich carbides may be present on a limited number of boundaries.

High temperature annealing reduced Nb and N enrichments, although Nb and N were still detected at some grain boundaries. This indicates that annealing dissolves most, but not all, of the intergranular carbonitrides. In the annealed condition, transgranular cracking is dominant even after hydrogen precharging of the Auger samples. Apparently, the grain boundaries that tend to fail are those where some carbonitrides remain. AES elemental mapping showed that some grain boundaries in annealed EN82H are enriched with Cr and C, consistent with the AEM evidence of intergranular M_7C_3 and $M_{23}C_6$ precipitation.

The Ti-rich spots in Figure 14c correspond to TiN inclusions that form in the interdendritic regions and often pin grain boundaries. These intermediate-sized (~1 μm diameter) inclusions are not dissolved during annealing, but their morphology was changed. Specifically, Nb and C, as well as Ti and N, are present after annealing. This is consistent with the AEM analysis that clearly identified complex multi-phase inclusions in which the AlMgSi-rich oxide core serves as the nucleation site for TiN inclusions, which, in turn, serve as preferential nucleation sites for the NbC during the high-temperature anneal.

The S-rich regions found on grain boundaries correspond to MgS inclusions. Most grain boundaries contained a very limited number of sulfides (e.g., the map in Figure 14f shows a few sulfide particles), while a few boundaries exhibited a slightly higher density. Although annealing at 1093°C did not dissolve the MgS inclusions, relatively few were observed at grain boundaries due to boundary migration.

DISCUSSION

Differences in the mechanical properties and microstructures for the as-fabricated versus annealed welds, as summarized in Table 3, provide significant insight into the observed behavior of the welds and the cause of LTCP. The root cause of low temperature embrittlement appears to be the Nb,Ti-rich carbonitrides decorating grain boundaries in as-fabricated welds. Both AEM and AES studies show that these fine carbonitrides cover the majority of grain boundaries in the as-welded condition, which is susceptible to LTCP. Because these carbides

serve as effective hydrogen traps, they promote hydrogen-induced intergranular fracture in low temperature water.

The 1093°C anneal resulted in the dissolution of most of the ultra-fine (3-16 nm) Nb,Ti-rich M(C,N) precipitates, whereas the subsequent slow cooling promoted the intergranular precipitation of Cr-rich M_7C_3 and $M_{23}C_6$ carbides. These observations indicate that immunity to intergranular LTCP after annealing is associated with elimination (via dissolution) of the ultra-fine intergranular carbonitrides that appear to promote hydrogen embrittlement, and precipitation of chromium-rich M_7C_3 and $M_{23}C_6$ carbides that appear to provide resistance to LTCP. This is further supported by the observation of transgranular faceting in annealed specimens tested in 54°C water. The faceted cracking mode indicates that hydrogen from the water embrittled the matrix, but did not embrittle grain boundaries because dissolution of the fine Nb,Ti-rich M(C,N) precipitates enhanced their resistance to hydrogen embrittlement. Even after hydrogen precharging, most of the grain boundaries in the annealed weld resisted separation; the few grain boundaries that did fail were probably those where some carbonitrides remain.

The TiN inclusions that tend to pin grain boundaries may also degrade LTCP resistance if they serve as hydrogen traps; however, their presence in the annealed weld showed that by themselves they cannot induce intergranular cracking. Apparently, the low grain boundary coverage of inclusions is too sparse to cause grain boundary embrittlement in water.

Grain boundary segregation was suspected as promoting LTCP in EN82H because the nature of this cracking was similar to that for Alloy X-750 where P and S segregation was correlated with cracking susceptibility.[9] In the weld, however, grain boundary segregation does not appear to cause LTCP. There is no evidence of S segregation and the observed 1.4 atomic percent P segregation on half of the grain boundaries in the as-fabricated weld is not expected to be sufficient to promote low temperature cracking.

The intergranular MgS particles present in both the as-fabricated and annealed welds do not appear to play a dominant role in causing LTCP, although they may have some effect in local regions. Decomposition of MgS particles[10] when exposed to deaerated water produces sulfides in the crack tip environment, which are known to be detrimental to environmental cracking performance. However, the density of MgS particles is judged to be too low to impact

the crack tip chemistry. In regions where the sulfide density is particularly high, it is possible that their decomposition can influence cracking behavior, but this effect would be very localized.

AEM characterization revealed that the 1093°C anneal caused a significant reduction in the dislocation content, which accounts for the observed 50% reduction in yield strength. The higher yield strength for the as-fabricated weld is expected to promote LTCP because it increases both local stresses ahead of a crack and local hydrogen concentration in the peak triaxial stress region. However, the annealing and cold rolling studies clearly demonstrated that strength levels were not a primary cause of low temperature embrittlement. Specifically, the annealed and cold-rolled weld, with a yield strength comparable to that for the as-fabricated weld, showed little or no embrittlement in hydrogenated water and there was no evidence of intergranular cracking. This finding clearly demonstrates that the absence of intergranular cracking in both the annealed and annealed and cold-rolled conditions is associated with differences in grain boundary structure, rather than differences in strength.

The different environmental responses exhibited by the annealed versus annealed and cold-rolled welds are believed to be associated with markedly different dislocation structures. In the annealed condition, values of J_{IC} and T obtained in 54°C water were reduced by about 50% due to a hydrogen-induced transgranular faceting mechanism. The annealed and cold-rolled weld showed a smaller environmental effect (J_{IC} and T were reduced by about 20%) and the fracture mode was predominantly dimple rupture with limited evidence of faceting. Differences in the initial dislocation structures for the two conditions are apparently responsible for the different cracking responses. Specifically, the low density of dislocations in the annealed condition allows intense planar slip bands to form during straining in water. Separation along these planar slip bands produces the crystallographic facets and a modest reduction in toughness. By contrast, cold rolling the annealed weld generates a uniform dislocation network that fosters more homogeneous deformation during subsequent straining in water. The homogeneous nature of slip promotes microvoid coalescence and minimizes environment effects.

CONCLUSIONS

Susceptibility to intergranular LTCP in 54°C water causes a severe toughness loss in as-fabricated EN82H welds. Annealing the weld at 1093°C eliminated hydrogen-induced intergranular cracking in low temperature water and restored significant cracking resistance.

Mechanical property and microstructural studies were performed to identify the key features responsible for LTCP; conclusions drawn from these studies are summarized below:

- The key microstructural feature responsible for LTCP in the as-fabricated weld appears to be the ultra-fine Nb and Ti-rich carbonitrides that were present at most grain boundaries. These precipitates are effective hydrogen traps that promote hydrogen-induced intergranular cracking.

- Annealing at 1093°C dissolved most of the ultra-fine carbonitrides, which accounts for the observed immunity to intergranular cracking in low-temperature water.

- High strength levels can promote intergranular LTCP in susceptible materials because they increase both local stresses and hydrogen concentrations ahead of a crack. However, the annealed and cold-rolled weld, with a high yield strength, showed no evidence of hydrogen-induced intergranular cracking in water, thereby demonstrating that strength alone is not a root cause of low-temperature embrittlement.

ACKNOWLEDGEMENT

This work was performed under U. S. Department of Energy Contract DE-AC11-98PN38206 with Bettis Atomic Power Laboratory. The electron microprobe analyses were obtained via subcontract to R. J. Lee Group, Inc. and AES evaluations were obtained via subcontract to Materials Research Laboratories, Inc.

REFERENCES

1. C. M. Brown and W. J. Mills, "Effect of Water on Mechanical Properties and Stress Corrosion Behavior of Alloy 600, Alloy 690, EN82H Welds and EN52 Welds," *Corrosion*, Vol. 55, 1999, pp. 173-186.

2. W. H. Bamford, J. P. Foster and R. S. Pathania, "An Investigation of Alloy 182 Stress Corrosion Cracking in Simulated PWR Environment," *Ninth International Symposium on Environmental Degradation of Materials in Nuclear Power Systems-Water Reactors*, TMS, 1999, pp. 279-296.

3. L. G. Ljungberg, A. Ortnas, P. Stahle and J. L. Nelson, "Stress Corrosion Cracking Initiation in Alloys 600 and 182," *Sixth International Symposium on Environmental Degradation of Materials in Nuclear Power Systems-Water Reactors*, TMS, 1993, p. 379-386.

4. W. J. Mills and C. M. Brown, "Fracture Behavior of Nickel-Based Alloys In Water," *Ninth International Symposium on Environmental Degradation of Materials in Nuclear Power Systems-Water Reactors*, TMS, 1999, pp. 167-177.

5. W. J. Mills and C. M. Brown, "Fracture Toughness of Alloy 600 and EN82H Welds in Air and Water," *Metallurgical and Materials Transactions A*, in press (Report B-T-3264).

6. W. C. Porr and W. J. Mills, "Application of the Normalization Data Analysis Technique for Single Specimen R-Curve Determination," Bettis Atomic Power Laboratory, Report B-T-3269, February 1999.

7. P. C. Paris, H. Tada, A. Zahoor and H. Ernst, "The Theory of Instability of the Tearing Mode for Elastic-Plastic Crack Growth," *Elastic-Plastic Fracture*, ASTM STP 668, 1979, pp. 5-36.

8. M. G. Burke, R. J. Wehrer, and C. M. Brown, "Real-World Microscopy: Understanding the Environment-Sensitive Behavior of Ni-Base Welds", *Microscopy & Microanalysis,* Vol. 4, 1998, pp. 528-529.

9. W. J. Mills, M. R. Lebo and J. J. Kearns, "Hydrogen Embrittlement, Grain Boundary Segregation and Stress Corrosion Cracking of Alloy X-750 in Low and High Temperature Water," *Metallurgical and Materials Transactions*, Vol. 30A, 1999, pp. 1579-1596

10. *CRC Handbook of Chemistry and Physics*, 77th Edition, CRC Press, Inc., 1996, pp. 4-69 and 8-96.

Table 1. Average Tensile Properties for EN82H Weld at Room Temperature

Condition	σ_{YS} (MPa)	σ_{UTS} (MPa)	Elongation (%)
As-welded	600	810	26
Annealed	280	710	43
Annealed and cold-rolled	640	830	32

Table 2
Grain Boundary Composition (in Atomic Percent ± Standard Deviation) for As-fabricated and Annealed EN82H Welds. †
Composition of Transgranular Cracked Regions Are Provided for Comparison Purposes.

Material/ Condition	Regions Interrogated	B	N	Al	P	S	Ti	Cr	Mn	Fe	Ni	Nb
As-welded	13 GBs‡	1.3 ± 0.7	2.5±0.4+ 1.5±0.5+	0.9 ± 0.3	1.4±0.3* 0.6±0.2*	0.7 ± 0.4	1.2 ± 0.3	15.2 ± 2.2	1.8 ± 1.2	2.0 ± 1.3	62.2 ± 7.0	19.2±2.0* 7.6±2.4*
Annealed	5 GBs‡	1.0 ± 0.7	0.9 ± 0.8	0. 8 ± 0.5	0. 8 ± 0. 5	0. 7 ± 0.3	1.2 ± 0.2	18.6 ± 2.2	0.9 ± 0.5	1.9 ± 0.9	66.7 ± 5.3	6.8 ± 4.7
As-welded & Annealed	13 TG Regions‡	1.3 ± 0.5	0.7 ± 0.5	1.0 ± 0.5	0.5 ± 0.3	0.5 ± 0.2	1.0 ± 0.1	19.5 ± 1.4	0.8 ± 0.4	2.1 ± 0.9	69.2 ± 2.1	3.8 ± 1.4

* Mean and standard deviation values are determined for high and low concentration groups.
+Separate N concentrations are determined in regions with high and low Nb concentrations.
† Note that values below about 0.5 to 1 a/o are probably not significantly different from 0.
‡ GB = Grain Boundary; TG = Trangranular Region

Table 3
Microstructural & Mechanical Properties for As-welded & Annealed EN82H Welds. Key Differences Are in Bold.

As-welded	**Annealed**
General Microstructure	
• Coarse dendritic grains. • Cored structure with enriched Nb + Mn in interdendritic regions.	• Recrystallized grains; some dendritic grains. • Reduced Nb & Mn enrichment.
Grain Boundary (GB) Segregation	
• No S segregation. • Limited P segregation.	• No segregation.
Intergranular Precipitates	
• **Nb,Ti(C,N) [3-16 nm] on most GBs.** • Few TiN inclusions on GB. • Very few MgS on GB.	• Nb,Ti(C,N) limited to nonrecrystallized GB. • **Cr-rich M_7C_3 & $M_{23}C_6$ on GB.** • Few TiN/Nb(C,N) inclusions on GB. • Extremely few MgS on GB.
Intragranular Precipitates & Inclusions	
• Nb,Ti(C,N) ppt [3-16 nm] on dislocations. • TiN inclusions • AlMgSi-rich oxides	• Nb,Ti(C,N) ppt [<200 nm] • Multiphase TiN/Nb(C,N) inclusions • AlMgSi-rich oxides
Dislocation Content	
• High density of dislocation tangles & networks	• Low density of dislocations, except in isolated nonrecrystallized regions.
Mechanical Properties	
σ_{YS} = **620 MPa** σ_{UTS} = 810 MPa Elong. = 26%	σ_{YS} = **280 MPa** σ_{UTS} = 710 MPa Elong. = 43%

Figure Captions

Figure 1. Effect of low temperature water on the fracture toughness of EN82H welds in the as-welded, 1093°C annealed, and 1093°C annealed and cold-rolled conditions. Values of T are given above each bar.

Figure 2. SEM fractographs showing (a) intergranular fracture in as-fabricated weld tested in 54°C water, (b) crystallographic facets and poorly defined dimples in annealed weld tested in 54°C water, and (c) high magnification of crystallographic facets in (b).

Figure 3. SEM fractographs of annealed and cold-rolled weld tested in 54°C water showing: (a) well-defined dimples and a few crystallographic facets steeply inclined to loading axis, and (b) high magnification of well-defined dimples.

Figure 4. Light optical micrographs showing general structure of as-fabricated weld. (a) Grain boundaries separate colonies of similarly oriented dendrites. (b) Note the undulating nature of grain boundaries as interdendritic inclusions tend to pin boundaries.

Figure 5. SEM micrographs of as-fabricated weld (etched). (a) Undulating nature of grain boundaries. TiN inclusions within interdendritic regions sometimes pin grain boundaries. (b) Agglomerated clusters of Nb,Ti-rich precipitates along shallow section of grain boundary.

Figure 6. Light optical micrographs showing general structure of annealed weld. (a) Recrystallized, equiaxed grains with numerous annealing twins. (b) Localized regions of coarse dendritic grains (upper left) surrounded by recrystallized grains.

Figure 7. SEM micrographs of annealed weld. (a) Unrecrystallized region with undulating grain boundaries (right) and recrystallized region with annealing twins (left). (b) Coarsened precipitates decorate grain boundaries in unrecrystallized region.

Figure 8. Transmission electron micrograph showing general dislocation structure of as-fabricated weld.

Figure 9. Dark-field transmission electron micrographs of as-fabricated weld showing (a) fine (~3-16 nm) NbTi(CN) precipitates decorating grain boundaries, and (b) fine intergranular NbTi(CN) precipitates and discrete intragranular carbonitrides decorating pre-existing dislocations.

Figure 10. Transmission electron micrograph of annealed weld showing a greatly reduced dislocation density and presence of Nb,Ti(CN) inclusions.

Figure 11. Intergranular carbide morphology for 1093°C annealed weld. (a) Secondary electron micrographs showing the presence of M_7C_3 at grain boundaries. (b) Transmission electron micrograph of intergranular $M_{23}C_6$ carbides. Inset: [110] selected area electron diffraction pattern showing cube-on-cube orientation relationship between the semicoherent $M_{23}C_6$ and fcc matrix.

Figure 12. Transmission electron micrographs of multi-phase inclusion in annealed weld. (a) Bright-field and (b) dark-field images showing the AlMgSi-rich oxide inclusion core surrounded by a TiN inclusion that served as nucleation site for NbC precipitation.

Figure 13. Transmission electron micrographs of an unrecrystallized region within annealed weld. (a) Bright-field image showing dislocation substructure in region with coarsened Nb-rich carbonitrides that inhibited recrystallization. (b) Dark-field image of the coarsened carbonitrides.

Figure 14. AES elemental distribution map of as-fabricated weld. (a) Secondary electron fractograph showing intergranular fracture surface interrograted by AES. (b)-(f) Elemental distribution maps for C, Ti, Nb, Cr and S.

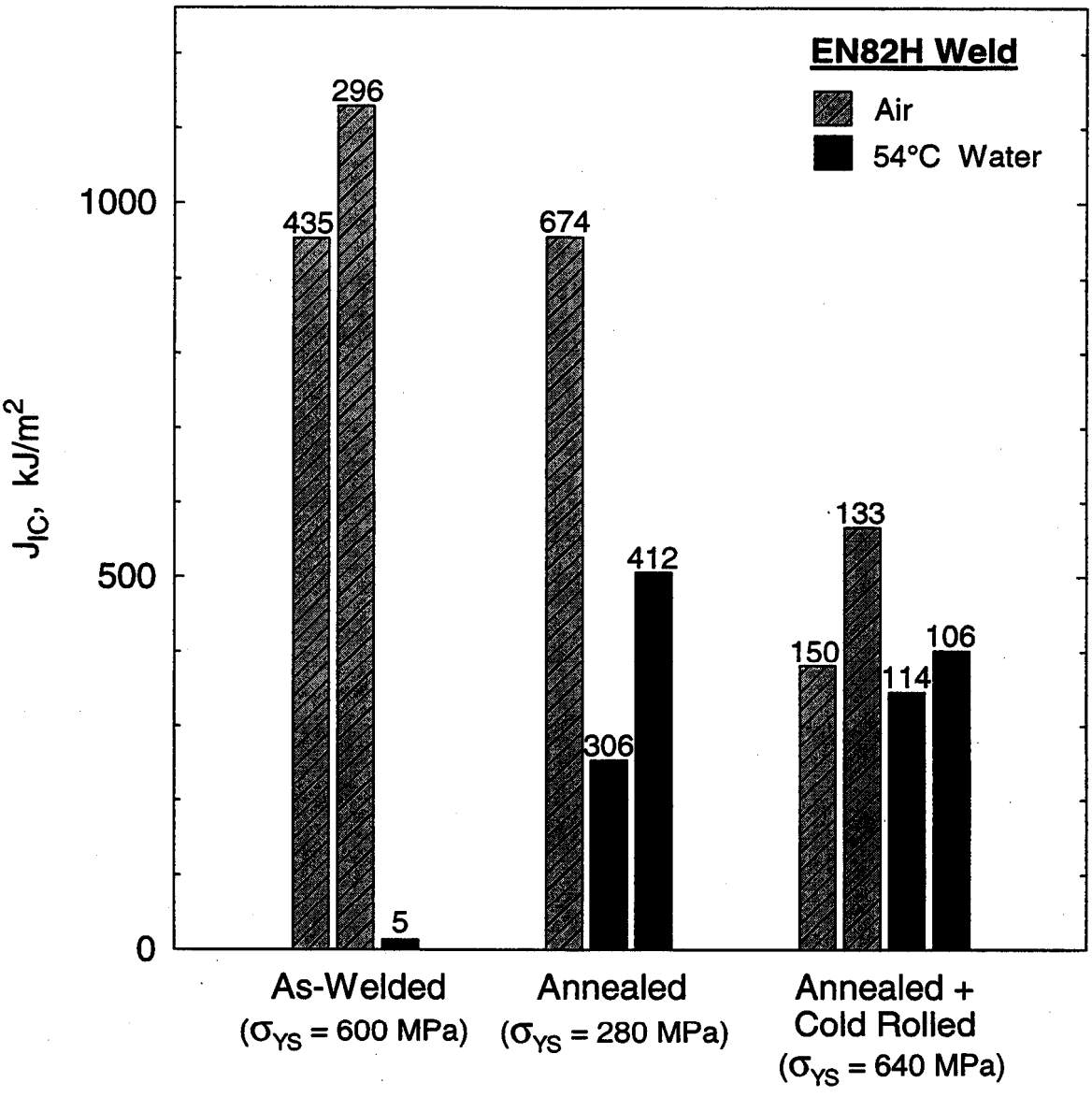

Figure 1. Effect of low temperature water on the fracture toughness of EN82H weld in the as-welded, 1093°C annealed, and 1093°C annealed + cold rolled conditions. Values of T are given above each bar.

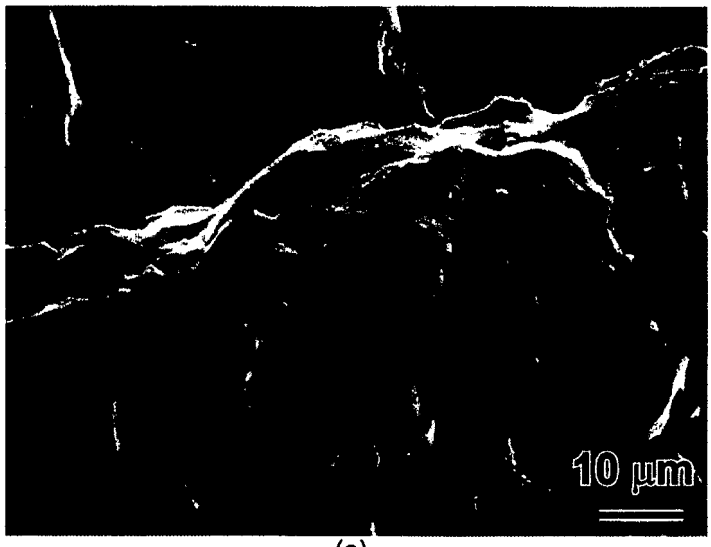

(a)

(b)

(c)

Figure 2. SEM fractographs showing (a) intergranular fracture in as-fabricated weld tested in 54°C water, (b) crystallographic facets and poorly defined dimples in annealed weld tested in 54°C water, and (c) high magnification of crystallographic facets in (b).

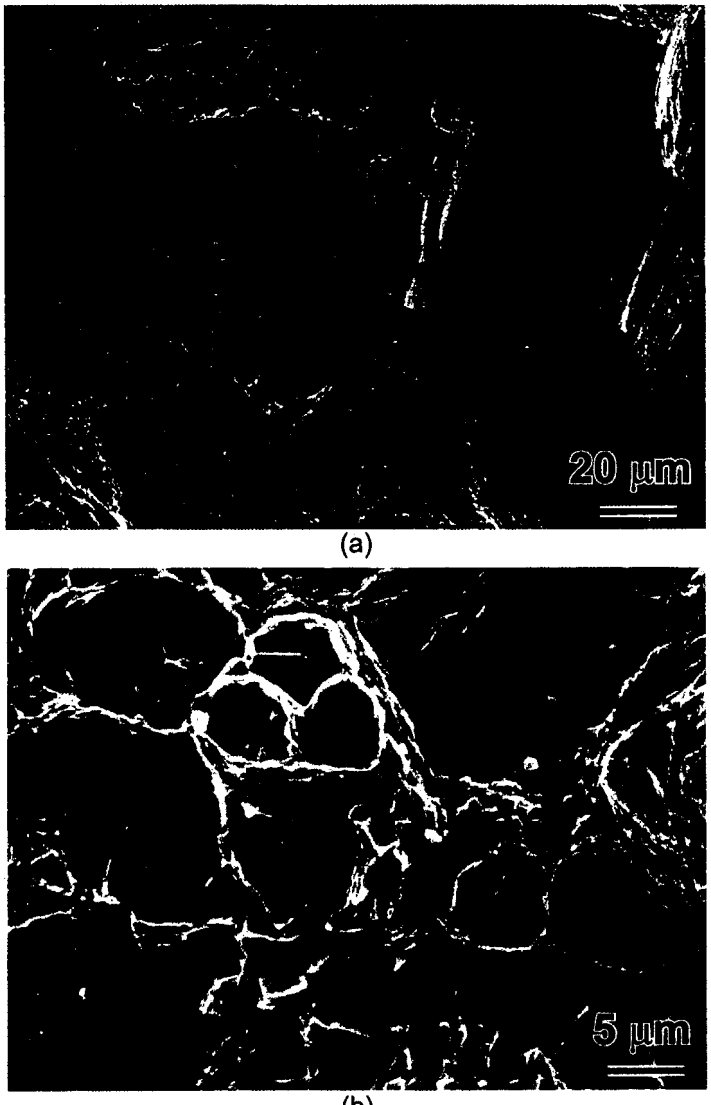

Figure 3. SEM fractographs of annealed and cold-rolled weld tested in 54°C water showing: (a) well-defined dimples and a few crystallographic facets steeply inclined to loading axis, and (b) high magnification of dimples.

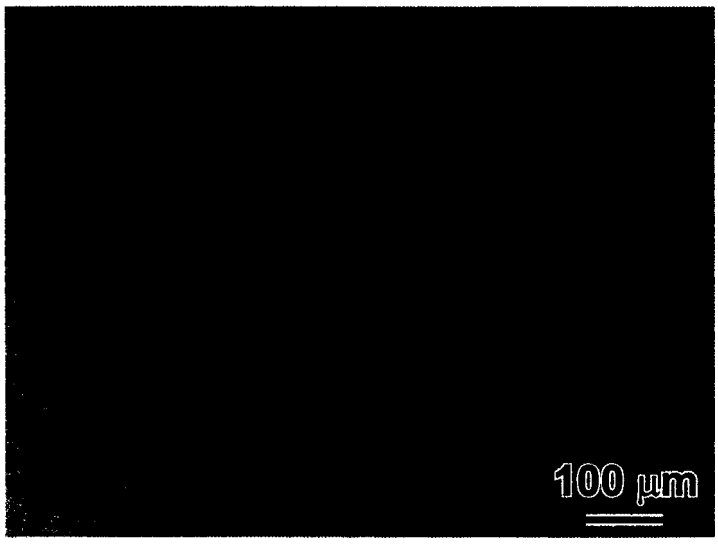

(a)

(b)

Figure 4. Light optical micrographs showing general structure of as-fabricated weld. (a) Grain boundaries separate colonies of similarly oriented dendrites. (b) Note the undulating nature of grain boundaries as interdendritic inclusions tend to pin boundaries.

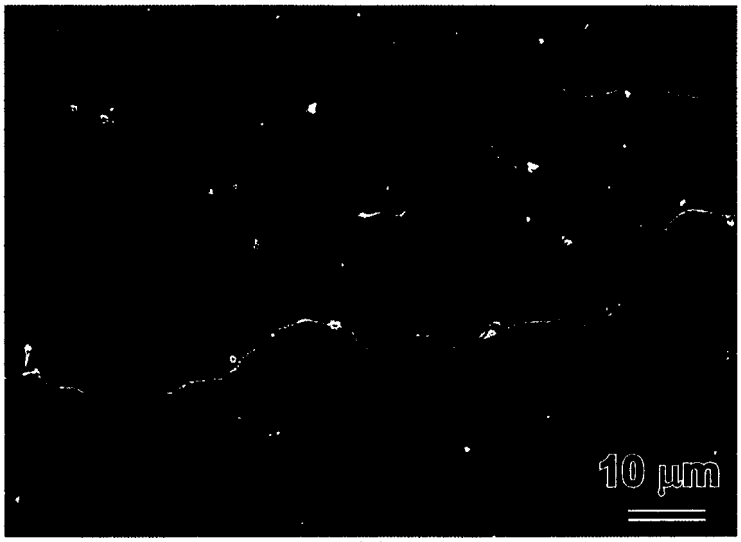

(a)

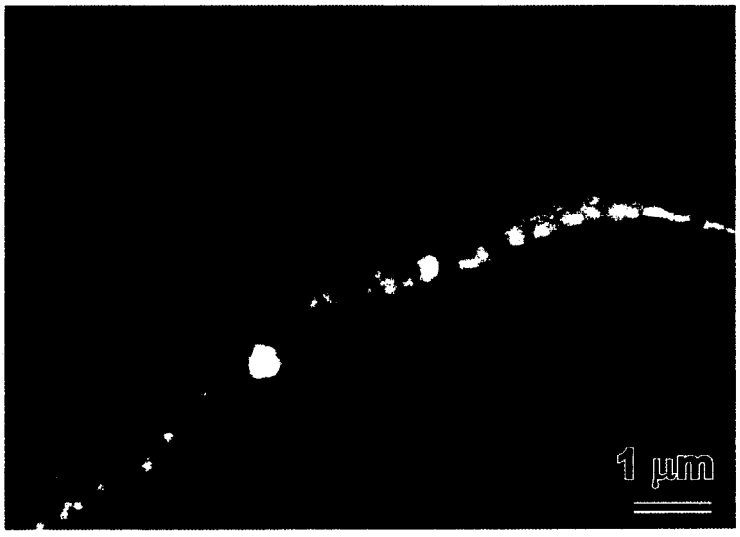

(b)

Figure 5. SEM micrographs of as-fabricated weld (etched). (a) Undulating nature of grain boundaries. TiN inclusions within interdendritic regions sometimes pin grain boundaries. (b) Clusters of fine Nb,Ti(C,N) precipitates along shallow section of grain boundary.

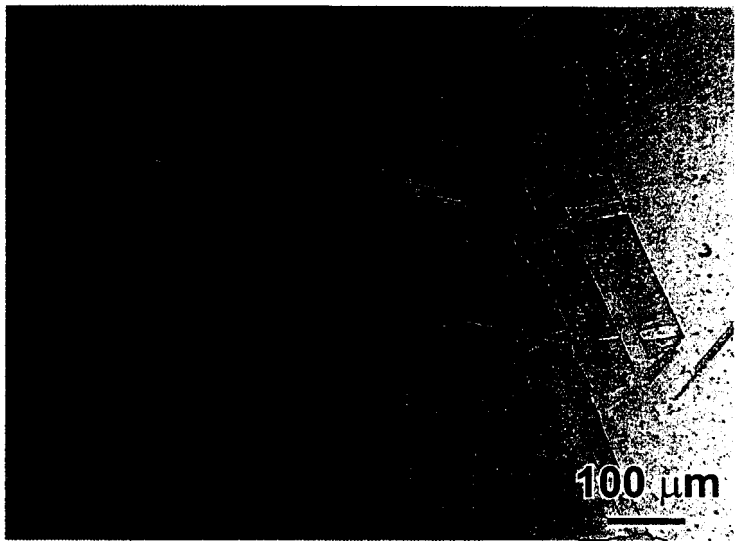

(a)

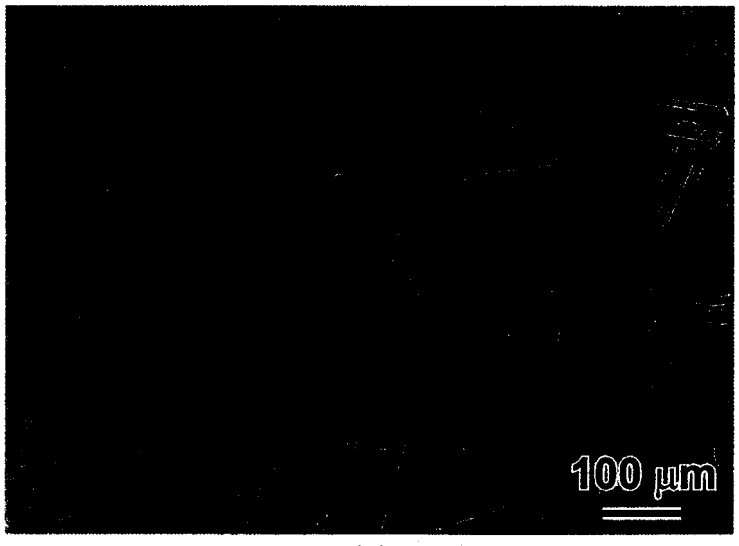

(b)

Figure 6. Light optical micrographs showing general structure of annealed weld. (a) Recrystallized, equiaxed grains with many annealing twins. (b) Localized region of coarse dendritic grains (upper left) surrounded by recrystallized grains.

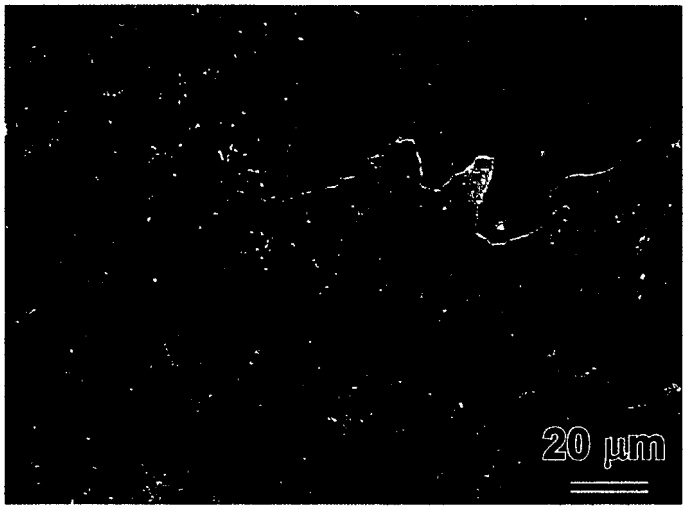

(a)

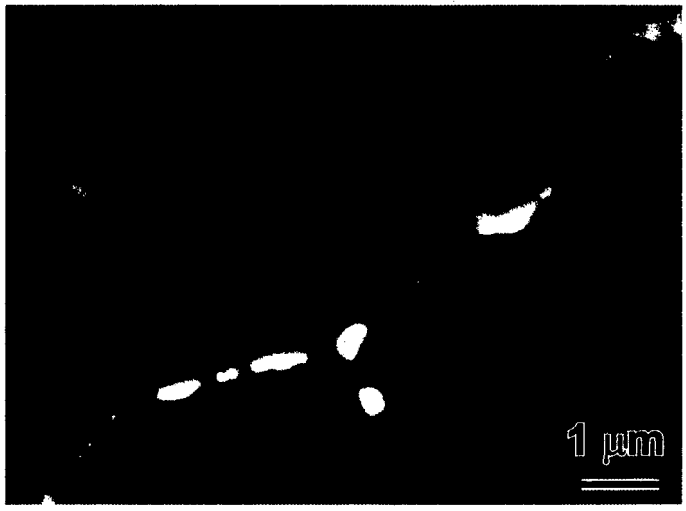

(b)

Figure 7. SEM micrographs of annealed weld. (a) Unrecrystallized region with undulating grain boundaries (right) and recrystallized region with annealing twins (left). (b) Coarsened precipitates decorate grain boundaries in unrecrystallized region.

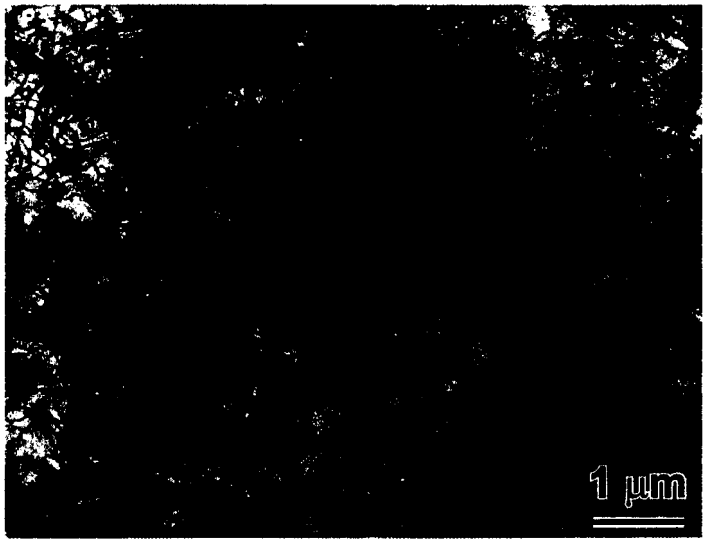

Figure 8. Transmission electron micrograph showing general dislocation structure of as-fabricated weld.

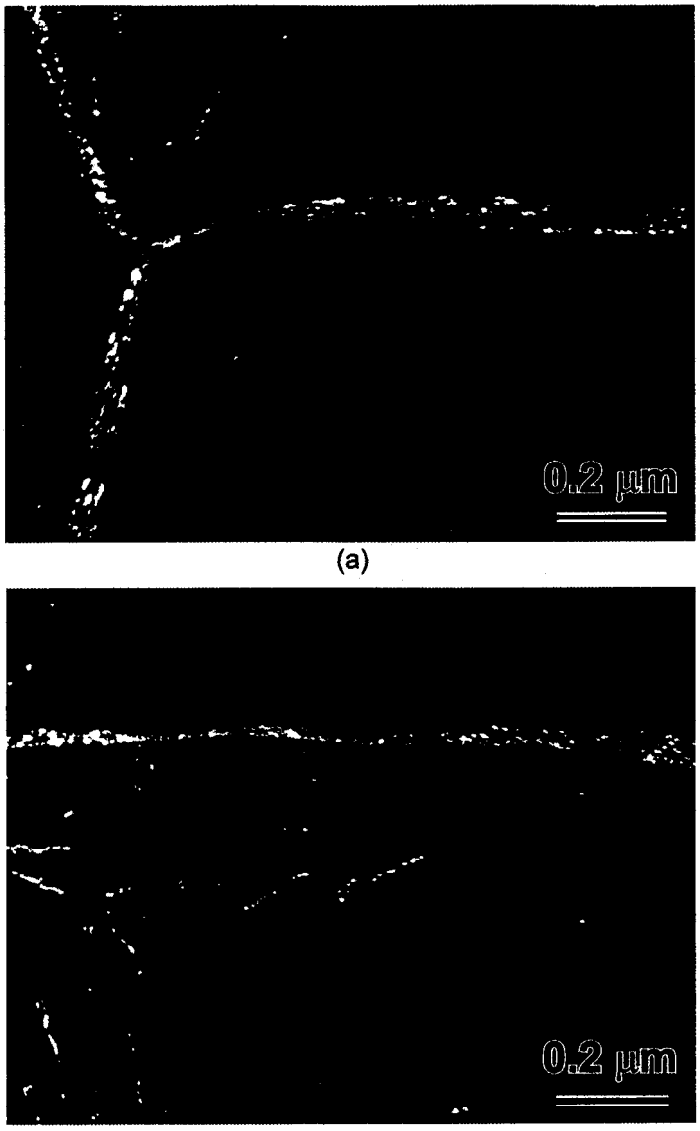

Figure 9. Dark-field transmission electron micrographs of as-fabricated weld showing (a) fine (3-16 nm) Nb,Ti(C,N) precipitates decorating grain boundaries, and (b) fine intergranular Nb,Ti(C,N) precipitates and discrete intragranular carbonitrides at pre-existing dislocations.

Figure 10. Transmission electron micrograph of annealed weld showing low dislocation density and presence of Nb,Ti(C,N) inclusions.

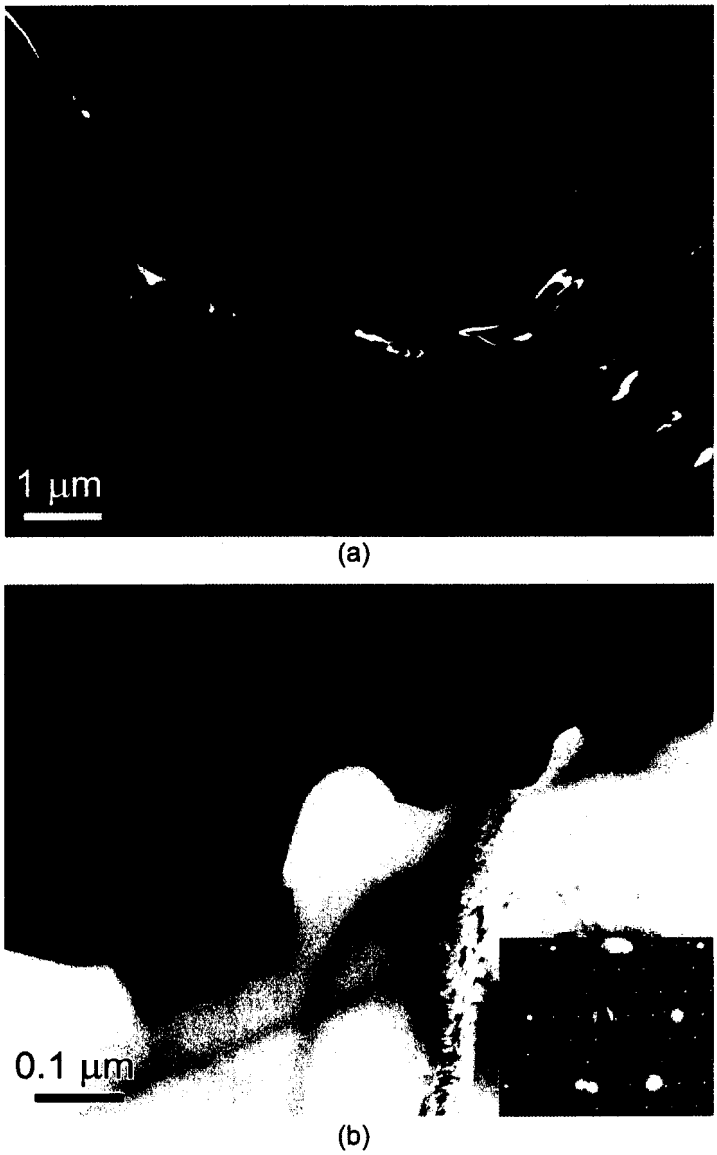

Figure 11. Intergranular carbide morphology for 1093°C annealed weld. (a) Secondary electron micrographs showing extensive M_7C_3 coverage of grain boundaries. (b) Transmission electron micrograph showing intergranular $M_{23}C_6$ carbides. Inset: [110] selected area electron diffraction pattern showing cube-on-cube orientation relationship between semicoherent $M_{23}C_6$ and fcc matrix.

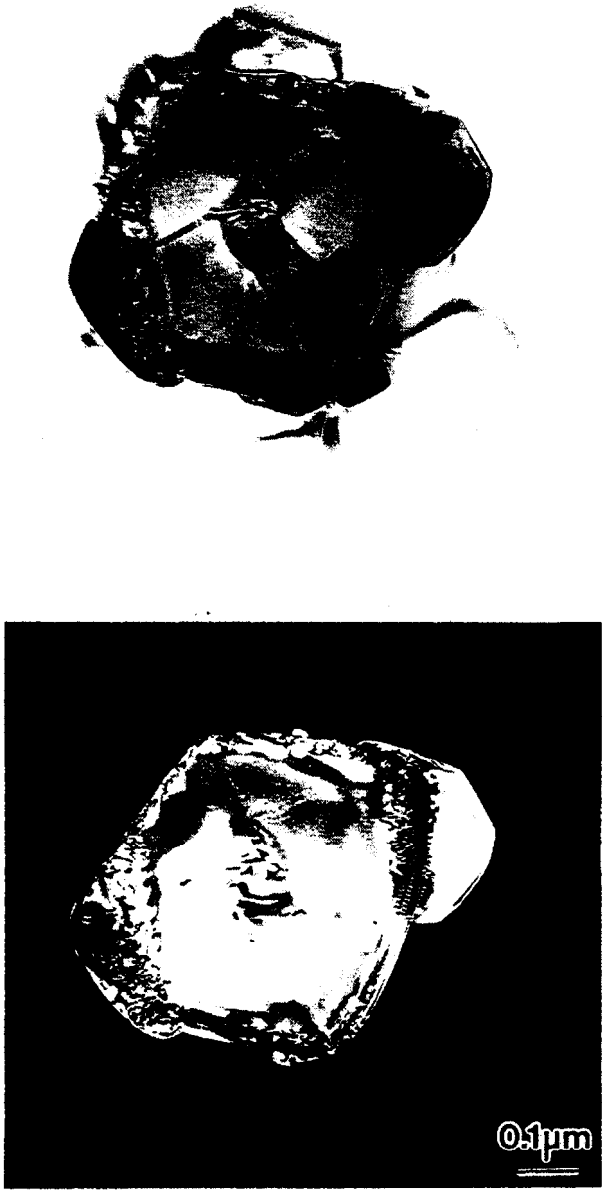

Figure 12. Transmission electron micrographs of multi-phase inclusion in annealed weld. (a) Bright-field and (b) dark-field images showing the AlMgSi-rich oxide inclusion core surrounded by a TiN inclusion that served as nucleation site for NbC precipitation.

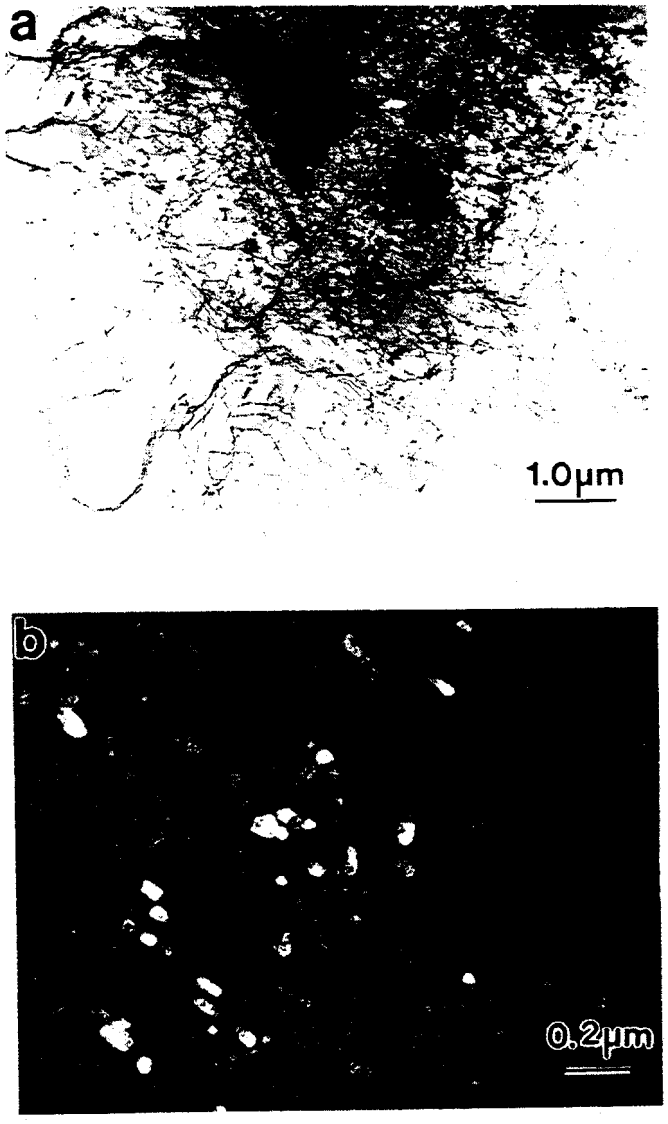

Figure 13. Transmission electron micrographs of an unrecrystallized region within annealed weld. (a) Bright-field image showing dislocation substructure in region with coarsened Nb-rich carbonitrides that inhibited recrystallization. (b) Dark-field image of the coarsened carbonitrides.

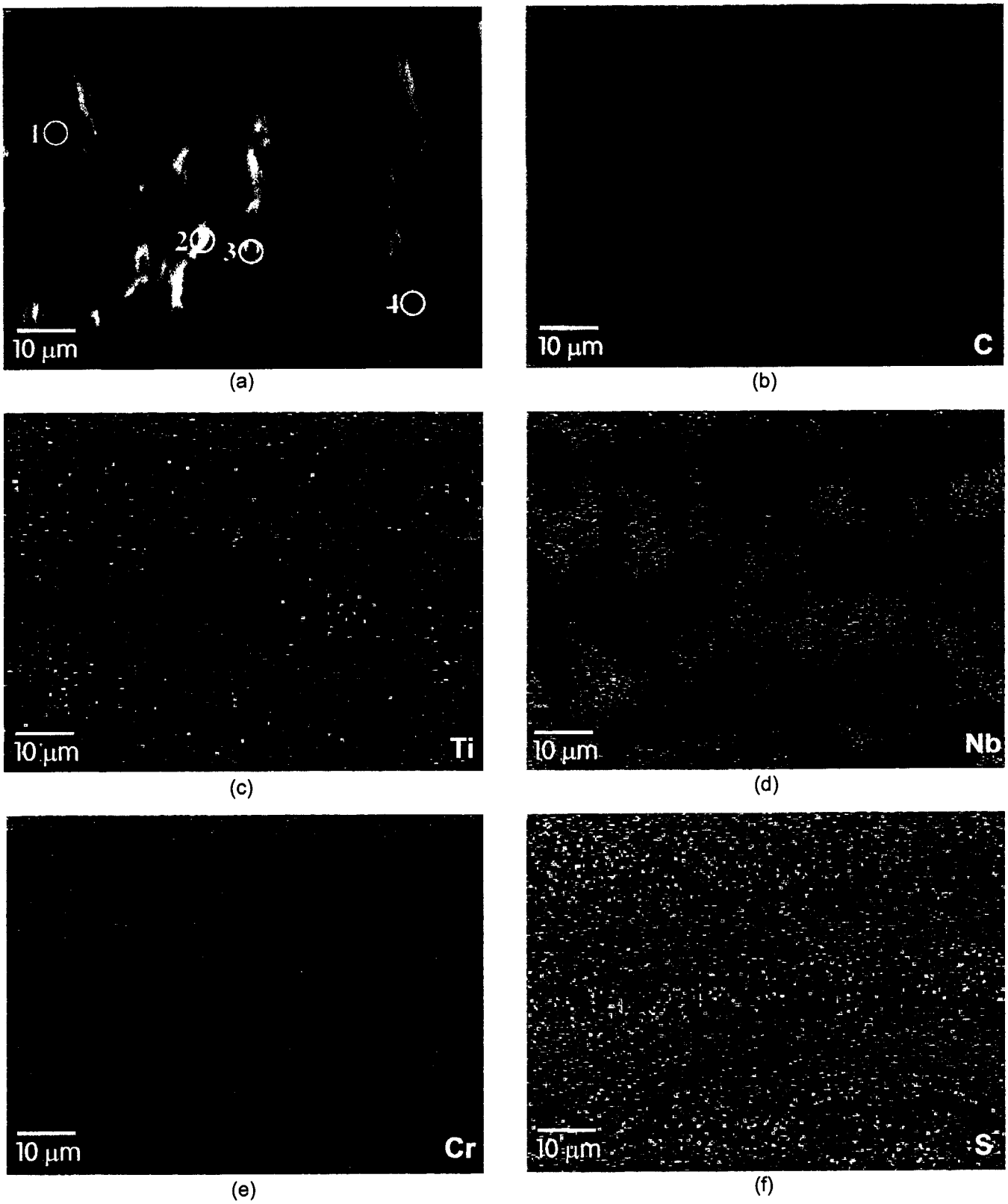

Figure 14. AES elemental distribution maps of as-fabricated weld. (a) Secondary electron fractograph showing intergranular fracture surface interrogated by AES. (b)-(f) Elemental distribution maps for carbon, titanium, niobium, chromium and sulfur.